GEOCHEMISTRY

A 160,000-year-old history of tectonically controlled methane seepage in the Arctic

Tobias Himmler[1,2]*, Diana Sahy[3], Tõnu Martma[4], Gerhard Bohrmann[5], Andreia Plaza-Faverola[2], Stefan Bünz[2], Daniel J. Condon[3], Jochen Knies[1,2], Aivo Lepland[1,2,4]

Copyright © 2019 The Authors, some rights reserved; exclusive licensee American Association for the Advancement of Science. No claim to original U.S. Government Works. Distributed under a Creative Commons Attribution NonCommercial License 4.0 (CC BY-NC).

The geological factors controlling gas release from Arctic deep-water gas reservoirs through seabed methane seeps are poorly constrained. This is partly due to limited data on the precise chronology of past methane emission episodes. Here, we use uranium-thorium dating of seep carbonates sampled from the seabed and from cores drilled at the Vestnesa Ridge, off West Svalbard (79°N, ~1200 m water depth). The carbonate ages reveal three emission episodes during the Penultimate Glacial Maximum (~160,000 to 133,000 years ago), during an interstadial in the last glacial (~50,000 to 40,000 years ago), and in the aftermath of the Last Glacial Maximum (~20,000 to 5,000 years ago), respectively. This chronology suggests that glacial tectonics induced by ice sheet fluctuations on Svalbard mainly controlled methane release from Vestnesa Ridge. Data corroborate past methane release in response to Northern Hemisphere cryosphere variations and suggest that Arctic deep-water gas reservoirs are sensitive to temperature variations over Quaternary time scales.

INTRODUCTION

Marine sediments north of the Arctic Circle contain three times more energy-equivalent gas than oil, estimated to be ~22×10^{12} m^3 of undiscovered gas (*1*). A large amount of the gas is stored along continental shelves in a water depth of less than ~500 m where tectonic and surface processes, and implicitly gas release, are controlled by the waxing and waning of Quaternary ice sheets (*2*, *3*). By comparison, the geological factors controlling seabed gas release at sites with water depths greater than 1000 mbsl (meters below sea level) over glacial-interglacial time scales are not well understood. Methane leaking from these reservoirs migrates along faults and gets partly sequestered as gas hydrate, which is stable within sediments at water depths below ~200 (high latitudes) to ~500 m in the gas hydrate stability zone (GHSZ) (*4*, *5*). If the pore fluid composition or temperature and pressure conditions do not favor hydrate formation, then methane can migrate through the sedimentary column, eventually emanating at seafloor seeps (*6*). However, before entering the ocean, microbially mediated anaerobic oxidation of methane (AOM) consumes up to 90% of the methane near the sediment-water interface (*7*, *8*). Besides sulfate-driven AOM ($CH_4 + SO_4^{2-} \rightarrow HCO_3^- + HS^- + H_2O$) (*7*), AOM can also be coupled with iron and manganese reduction using iron oxyhydroxide and manganese oxide as electron acceptors (*9*). A consequence of AOM is the production of bicarbonate (HCO_3^-), which increases the pore-fluid alkalinity and facilitates the precipitation of authigenic seep carbonates (*10*, *11*). Seep carbonates are amenable to radioisotopic dating using the uranium-thorium (U-Th) isotope system, providing a precise temporal record of past methane seepage from which the geological factors controlling methane release may be inferred (*12*–*14*).

Methane seeps are abundant along the Norwegian continental margin, including the Barents Sea (~340 mbsl) (*15*), offshore West Svalbard (~30 to ~430 mbsl) (*16*), and at Vestnesa Ridge (~1200 mbsl; Fig. 1) (*17*). Vestnesa Ridge is a ~100-km-long and up to 5-km-thick northwest (NW)–southeast (SE)–oriented drift comprising late Miocene to Holocene sediments (*17*). Acoustic anomalies pinpoint the base of the GHSZ around 200 mbsf (meters below seafloor) (*17*). Free gas is present in the sediment below 200 mbsf, ascending through gas chimneys along subvertical faults and fractures cross-cutting the GHSZ to be released into the ocean at episodically active seeps on the ridge crest (*18*, *5*). U-Th dating of seep carbonates sampled from the seafloor at Vestnesa Ridge and shallower areas off West Svalbard and the southwest (SW) Barents Sea reveals widespread methane seepage since the Last Glacial Maximum (LGM) over the past ~23 ky (thousand years) (*19*, *13*, *14*). Seepage occurred in both shallow areas (<400 mbsl), where pressure release after the retreat of the grounded Scandinavian Ice Sheet led to gas hydrate destabilization (*14*), and at the deep-water Vestnesa Ridge, which has not been reached by the grounded ice sheet (*3*). Although methane seepage at Vestnesa Ridge is thought to have started ~2 million years ago based on seismic evidence (*5*) and basin modeling (*20*), the chronology of pre-LGM methane emission has not been constrained to date. As Vestnesa Ridge at ~1200 mbsl has not been affected by glacial erosion through grounded ice, pre-LGM seep carbonates were likely preserved in the sediment record. This makes Vestnesa Ridge an ideal locality to investigate the factors controlling long-term methane seepage on a climate-sensitive high-latitude continental margin at over 1000 mbsl.

This study identifies three major seepage episodes recorded by authigenic seep carbonates sampled from the seafloor using a remotely operated vehicle (ROV) and from two shallow drill cores down to ~23 mbsf using the seafloor drill rig MARUM-MeBo70 (Fig. 1, figs. S1 to S3, and Table 1) (*21*). As opposed to the inferred chronology based on seismic and modeling data, detailed seep carbonate U-Th dating (Fig. 2) confirms two pre-LGM seepage episodes, extending the Arctic methane seepage chronology beyond the Penultimate Glacial Maximum (PGM) ~140 thousand years ago (ka) (Fig. 3). Radioisotopic dating was complemented by macro- and

[1]Geological Survey of Norway, P.O. Box 6315 Torgarden, 7491 Trondheim, Norway. [2]Centre for Arctic Gas Hydrate, Environment and Climate, Department of Geosciences, UiT The Arctic University of Norway, Tromsø, Norway. [3]British Geological Survey, Keyworth, Nottingham NG12 5GG, UK. [4]Department of Geology, Tallinn University of Technology, Tallinn, Estonia. [5]MARUM–Center for Marine and Environmental Sciences and Department of Geosciences, University of Bremen, 28334 Bremen, Germany.
*Corresponding author. Email: tobias.himmler@ngu.no

Downloaded from http://advances.sciencemag.org/ on August 9, 2019

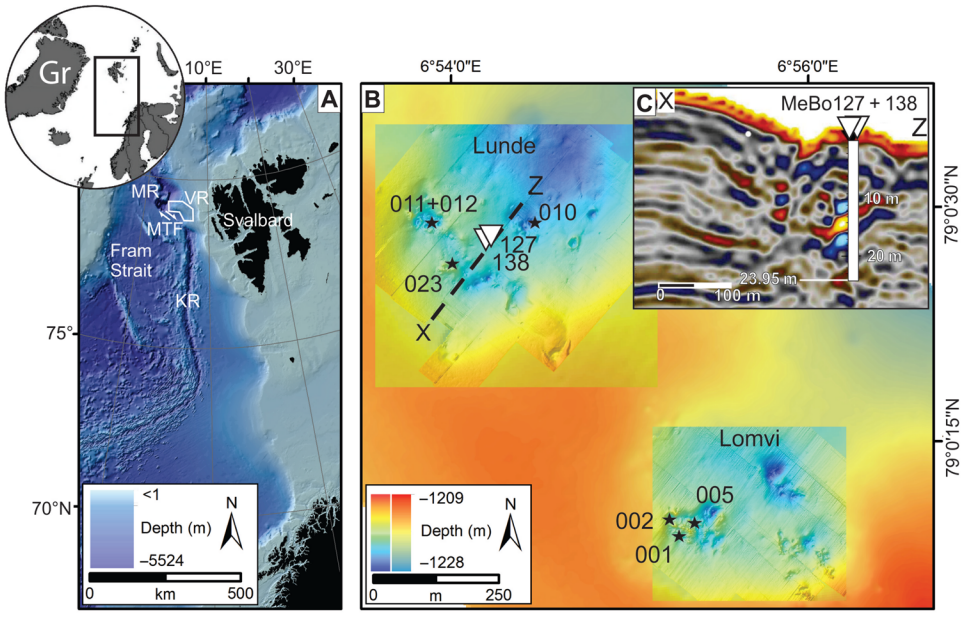

Fig. 1. Location and bathymetry of the sampling area. (**A**) Vestnesa Ridge (VR; white box) located in eastern Fram Strait, North Atlantic, northeast of the Molloy transform fault (MTF); KR, Knipovich Ridge; Gr, Greenland. Bathymetry from (*54*). (**B**) High-resolution bathymetry maps of the two sampled pockmarks over a low-resolution map, revealing multiple depressions and mounds within Lunde and Lomvi pockmarks. Stars indicate seabed samples (P1606001, P1606002, P1606005, P1606010, P1606011, P1606012, and P1606023). Triangles indicate drill sites of MeBo cores 127 (core GeoB21616-1) and 138 (core GeoB21637-1). The dashed line indicates seismic profile shown in (C). (**C**) Seismic profile across the SW sector of Lunde. Triangles indicate MeBo cores. The white vertical bar represents the maximum drilling depth of 23.95 m below seafloor, modified from (*21*). Note that the high-amplitude reflectors correspond to seep carbonates.

microscopic fabric description (fabric, figs. S4 to S8; radioisotopic data, figs. S9 and S10), compositional information derived from x-ray diffraction (tables S1 and S2), and carbonate stable isotope analyses ($\delta^{13}C$ and $\delta^{18}O$; data file S1).

RESULTS AND DISCUSSION

Seabed observations, core description, and carbonate fabric

Carbonates were sampled with the ROV from meter-scale mounds and meter- to decameter-scale depressions on the seafloor within two up to ~700-m-wide pockmarks previously named Lunde and Lomvi (Fig. 1). The seafloor next to the seep carbonates was frequently covered by meter-scale white and gray mats of putative sulfide-oxidizing bacteria (fig. S1). The microbial mats and bubbles emanating from the sediment during ROV sampling confirm active seepage and gas-charged sediment.

Subsurface seep carbonates have been previously inferred from seismic data (*22*) and were successfully drilled with two MeBo cores placed less than ~20 m apart within the central Lunde pockmark (Figs. 1 and 2). MeBo cores GeoB21616-1 and GeoB21637-1 reached maximum depths of 13.90 and 23.95 mbsf with sediment recoveries of 26 and 37%, respectively (Table 1). Given their proximity, the two cores were spliced into a composite record for description (Fig. 2 and figs. S2 and S3). The cored sediments comprise mainly silty clay with occasional glaciogenic gravel. Distinct authigenic carbonates occur between 5.75 and 22.53 mbsf. Abundant cracks and voids in the upper ~15 m of silty clay of GeoB21637-1 indicate gas expansion during core recovery. Core GeoB21616-1 contained ~4- and ~8-cm-thick massive seep carbonates embedded between loose carbonate gravel from 5.79 to 5.95 mbsf and a massive piece at 10.23 to 10.27 mbsf. Core GeoB21637-1 contained massive carbonate up to 13 cm thick and loose carbonate gravel between 16.95 and 22.53 mbsf.

Seabed and core carbonates comprise clast-supported breccias (figs. S4 to S6). Relatively early cemented sediment clasts have been subsequently cemented by later void-filling botryoidal and radial-fibrous aragonite (tables S1 and S2). Bivalve shells and gastropods are frequent bioclasts. Microcrystalline aragonite primarily cements the sediment matrix, but some samples comprise mainly microcrystalline Mg-calcite as matrix cement. Quartz, plagioclase, and clay minerals constitute the major noncarbonate components. Whereas some seabed samples contain abundant glaciogenic gravel, no noncarbonate grains larger than 2 mm in diameter have been observed in cored samples (figs. S4 to S8).

U-Th dating and methane seepage chronology

U-Th dating of 58 void-filling aragonite cement samples resulted in data that cover a range of ($^{230}Th/^{232}Th$) versus ($^{238}U/^{232}Th$) values similar to the values of seep carbonates from the Norwegian margin and from lower latitude seeps (fig. S9) (*23*–*26*, *12*, *14*). Calculated ages from ROV-collected and core seep carbonates display a general upward-younging trend, revealing three major methane emission episodes (Fig. 2 and fig. S10). The core carbonates were dated to ~160 to 133 ka (mean age, ~148 ka; $n = 15$) and ~50 to 40 ka (mean, ~43 ka; $n = 7$), corroborating two pre-LGM seepage episodes (Fig. 3). Seabed carbonates yielded U-Th ages between ~20 and 5 ka (mean, 13 ka; $n = 16$), consistent with previously reported post-LGM seepage (*19*). The ages of the core carbonates reflect seepage episodes ~100 ky apart. The age-depth relationship suggests that integrated net sediment accumulation rates are ~0.15 m/ky within the pockmark, assuming seep carbonate formation within the first decimeters below seabed under high methane flux. Dates from three stratigraphic

Downloaded from http://advances.sciencemag.org/ on August 9, 2019

Table 1. Detailed seabed sample locations and core sections containing seep carbonates. mbsf, meters below seafloor; R, rotary drilling; P, push coring; CC, core catcher; n.a., not applicable.

Sample/core	Latitude (°N)	Longitude (°E)	Pockmark	Water depth (m)	Max. coring depth (mbsf)	Core sections with seep carbonates (depth mbsf)
P1606001	79°0.1445′	06°55.308′	Lomvi	1206	n.a.	n.a.
P1606002	79°0.156′	06°55.278′	Lomvi	1204	n.a.	n.a.
P1606005	79°0.15′	06°55.386′	Lomvi	1203	n.a.	n.a.
P1606010	79°0.45′	06°54.47398′	Lunde	1210	n.a.	n.a.
P1606011	79°0.456′	06°53.958′	Lunde	1207	n.a.	n.a.
P1606012	79°0.462′	06°53.952′	Lunde	1207	n.a.	n.a.
P1606023	79°0.414′	06°54.07′	Lunde	1204	n.a.	n.a.
GeoB21616-1	79°0.418′	06°54.245′	Lunde	1210	13.90	2R (5.75 to 6.02); 4P–CC (10.16 to 10.27)
GeoB21637-1	79°0.426′	06°54.246′	Lunde	1209	23.95	10R–CC (16.95 to 17.09); 11R–CC (19.25 to 19.34); 12R–1 (21.60 to 21.73); 12R–2 (21.73 to 22.53)

intervals indicate carbonate precipitation and persistent methane flux episodes over ~20 ky.

An ~100-ky period has been previously suggested for deep-water seeps in non-Arctic settings. Seismic evidence has been used to infer that methane release along the central Norwegian margin (~750 mbsl) has occurred between ~160 to 125 ka and 25 to 18 ka (*27*). Likewise, an ~100-ky period was suggested for methane seepage in the Gulf of Guinea (~130 and ~30 ka; ~1100 mbsl) (*28*). Gas exsolution due to reduced hydrostatic pressure and sediment overpressure resulting from rapid sediment deposition in ice-proximal settings have been suggested as potential seepage drivers (*27*, *28*). On the basis of these time constraints and U-Th ages of seabed-sampled seep carbonates from other continental margins, it has been put forward that seepage was enhanced during falling and low-stand sea level ultimately related to the Late Quaternary cryosphere variations (*12*, *24*). However, the significance of different mechanisms remains poorly understood.

The ages derived from the core carbonates point to seepage when the global relative sea level was ~80 to 120 m below modern level, whereas the seabed samples ages indicate protracted seepage during rising relative sea level (fig. S11). Evidence for enhanced seepage during times of both low and high relative sea levels suggests that other geological factors besides sea-level fluctuations are controlling methane seepage at Vestnesa Ridge. Seismic data reveal gas chimneys feeding the active seabed seeps, which occur exclusively along NW-SE striking near-vertical normal faults that penetrate the entire thickness of the GHSZ (*5*, *18*). Given the proximity of Vestnesa Ridge, the repeatedly glaciated Svalbard archipelago, it is put forward that fault reactivation through glacial tectonics (*29*) plays a major role in controlling seepage over Quaternary time scales.

Deep methane drove shallow subsurface carbonate precipitation

The $\delta^{13}C_{carbonate}$ values for seabed samples range from −38.5 to −21.4 per mil (‰) (mean value ± 1σ: −31.5 ± 3.4‰; n = 49) and from −39.4 to −21.7‰ (−32.4 ± 3.1‰; n = 97) for core samples; the $\delta^{18}O$ values for seabed samples range from 4.6 to 6.4‰ (5.5 ± 0.4‰), and that for the core samples range from 4.0 to 6.6‰ (5.7 ± 0.6‰). For each sample, relatively early microcrystalline cement and later void-filling cement gave similar $\delta^{13}C$ and $\delta^{18}O$ values (fig. S12). The low $\delta^{13}C_{carbonate}$ values are typical of methane seep carbonates and point to AOM-induced carbonate precipitation (*30*, *10*, *11*). Methane seep carbonate $\delta^{13}C_{carbonate}$ values are ~10 to 25‰ higher than the parent methane $\delta^{13}C$ (*30*) because of admixture of relatively ^{13}C-enriched dissolved inorganic carbon (DIC) during carbonate precipitation [e.g., seawater DIC ≈ 0‰ Vienna Peedee belemnite (VPDB); DIC from the remineralization of organic matter ≈ −25‰ VPDB]. Assuming an admixture of ^{13}C-enriched DIC, the exclusively negative $\delta^{13}C_{carbonate}$ values between −39.4 and − 21.4‰ indicate that most DIC derived from the anaerobic oxidation of thermogenic methane ($\delta^{13}C_{methane}$ ≈ −50 to −20‰) (*31*). The $\delta^{13}C_{carbonate}$ values are consistent with $\delta^{13}C_{methane}$ values (−62.9 to −44.8‰ VPDB) and with long-term thermogenic methane release (*20*, *22*).

The $\delta^{18}O$ of seep carbonates depends largely on the carbonate-precipitating fluid $\delta^{18}O$ value and ambient temperature (*32*). When using the respective bottom-water temperatures for calculating the theoretical equilibrium $\delta^{18}O$, many samples yield $\delta^{18}O$ values indicative of precipitation from ^{18}O-enriched fluids (fig. S12). At seeps, enrichment of ^{18}O in the carbonate-precipitating fluid is caused by fluids affected by gas hydrate destabilization (*33*) and fluids affected by clay mineral dehydration in deeper sediments (*34*). Although these processes cannot be discriminated based on the $\delta^{18}O_{carbonate}$ values, a combination of both seems feasible for ^{18}O enrichment of the carbonate-precipitating pore fluid during seepage at Vestnesa Ridge. Episodic supply of deep-sourced and relatively warmer ^{18}O-enriched fluids ascending along faults (*18*, *20*) may cause local gas hydrate destabilization and liberation of ^{18}O-rich water and methane into shallow sediments. Modern shallow sediments show a higher thermal gradient within the active gas chimneys (95° and 85°C km^{-1}) compared to

Downloaded from http://advances.sciencemag.org/ on August 9, 2019

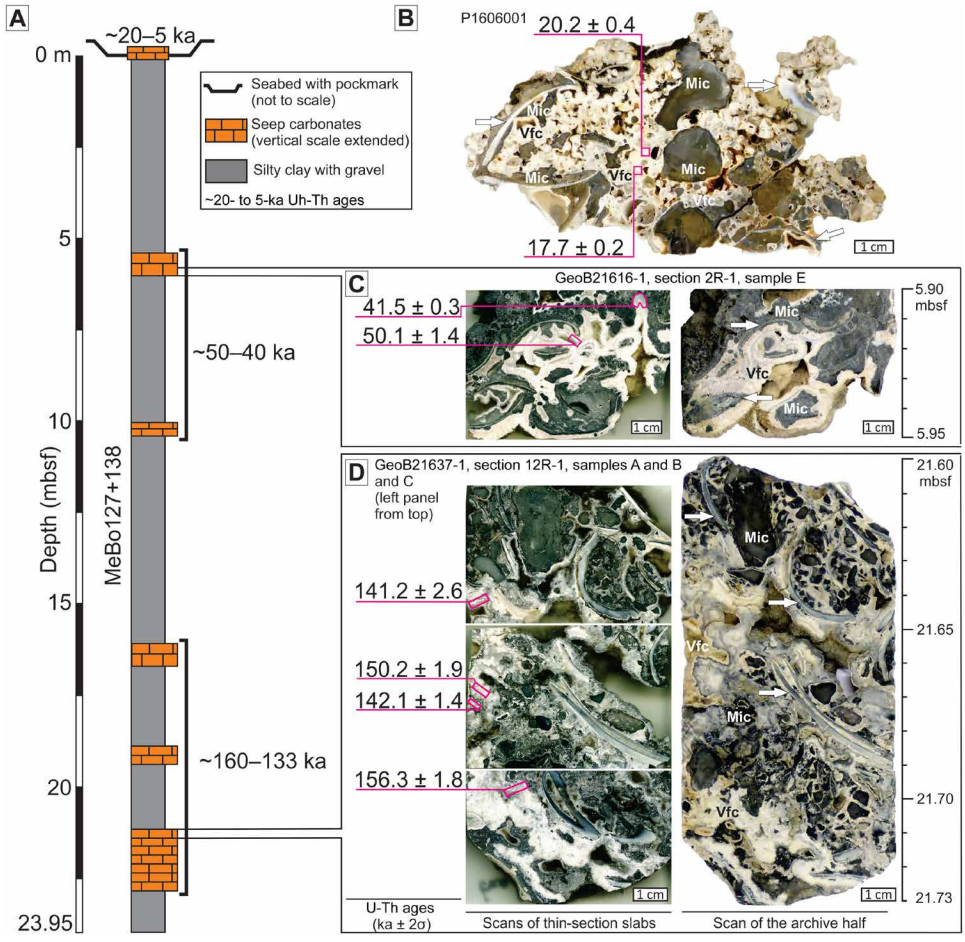

Fig. 2. Core lithology and representative seep carbonate samples with detailed U-Th ages (in ka ± 2σ). (**A**) Splice of adjacent MeBo cores 127 (core GeoB21616-1) and 138 (core GeoB21637-1) showing seabed and core samples and respective range of U-Th ages. Carbonate vertical scale is exaggerated for better visibility. (**B**) Scan of cut surface of seabed sample P1606001. (**C** and **D**) Scans of representative core samples. White arrows point to bivalve shells. Mic, microcrystalline carbonate cemented sediment; Vfc, void-filling cement.

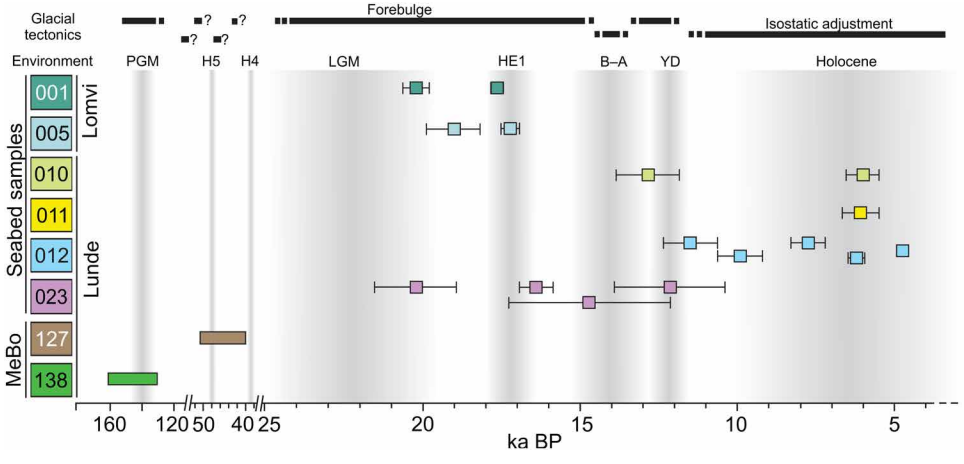

Fig. 3. Timing of seep carbonate formation (U-Th ages ± 2σ) relative to regional paleoclimate (vertical shaded bars) and glacial tectonics. U-Th ages obtained from seabed samples indicate multiple post-LGM methane seepage and associated carbonate formation. Ages obtained from core samples [samples 127 (GeoB21616-1) and 138 (GeoB21637-1)] reveal two pre-LGM seepage periods between ~160 to 133 ka and ~50 to 40 ka. Timing of seep carbonate formation and paleoclimate variations suggest glacial tectonics, i.e., forebulge movement and post-glacial isostatic adjustment as main geological drivers of episodic methane release from Vestnesa Ridge. H4 and H5, Heinrich stadials (cold); HE1, Heinrich event 1 (cold); B-A, Bølling-Allerød interstadial (warm); YD, Younger Dryas (cold).

Downloaded from http://advances.sciencemag.org/ on August 9, 2019

the surrounding sediment (76° and 75°C km^{-1}) (*21*), reflecting ascending warmer fluids.

Aragonite precipitation is favored over calcite close to the sediment-water interface, e.g., during vigorous emanation of methane bubbles and inflow of sulfate-rich seawater through the sediment disturbed by the strong fluid flow from below (*35*, *32*). In contrast, Mg-calcite precipitates under more restricted conditions when fluid flow is relatively weak (*32*). Under weak fluid flow conditions, AOM-produced hydrogen sulfide (HS^-) ions catalyze Mg-calcite precipitation by reducing the energy needed for dehydration of magnesium ions in the pore fluid (*36*). Regarding the brecciated carbonates cemented by microcrystalline aragonite and Mg-calcite cements, a shallow subsurface precipitation environment close to the sediment-water interface under increasing (i.e., weak to strong) methane flux is feasible. Processes leading to the formation of seep carbonate breccias include sediment seal and break due to excess pore pressure (*37*), sediment fracturing via gas hydrate growth and destabilization, and slumping of semi-lithified sediment (*32*). Considering that the carbonates were sampled on a ridge crest, gravitational slumping is unlikely, whereas vigorous methane release may account for the sediment brecciation. On the other hand, sediment disruption through growth and destabilization of shallow gas and associated vigorous methane release also leads to seep carbonate breccias. The relatively high carbonate $\delta^{18}O$ values suggest that the brecciated fabric is related to gas hydrate destabilization.

Glacial forebulge induced seepage during the PGM

The oldest cored carbonates reveal methane seepage during the PGM (Fig. 3). Given the water depth together with the long-lived methane supply from below, the sediment was likely prone to gas hydrate accumulation during this time. Assuming a water depth of ~1200 m minus the relatively lower PGM sea level (estimated to be ~120 m below the modern level) (*38*) places near-seabed sediments well within the GHSZ (*4*). Reduced hydrostatic pressure at PGM times caused by the lower sea level reduces the thickness of the GHSZ and may cause gas hydrate destabilization at the base of the GHSZ (*4*), releasing free gas and water into the sediment. It has been argued that, at Vestnesa Ridge, the effects of lower hydrostatic pressure caused by lower sea level (~120 m) and lower bottom-water temperatures (−1°C; i.e., colder environmental conditions) than at present cancel each other out (*39*). However, gas hydrate destabilization due to reduced hydrostatic pressure, as indicated by the brecciated carbonates and relatively high $\delta^{18}O_{carbonate}$ values, cannot be fully discarded. On the other hand, continuous seismic reflectors outside the paleo-pockmarks are indicative of undisturbed sediments, which suggest that hydrate destabilization was not widespread but was confined to the paleo-pockmarks. Enhanced heat transfer resulting from ascending deep-sourced fluids would have promoted hydrate destabilization exclusively within fault-bound sediments.

Previously, tectonic stress resulting from mid-ocean spreading has been suggested as a possible seepage driver at Vestnesa Ridge (*5*). In this study, fault reactivation through glacial tectonics is suggested as the main mechanism to bring deep fluids to the seabed during the PGM. Mantle viscosity modeling suggests the existence of a glacial forebulge off West Svalbard ~15, ~13, and ~11 ka resulting in a vertical lithosphere displacement of up to 60 m ca. 100 km seaward of the maximum ice extent during the LGM (*40*). Likewise, a glacial forebulge could have migrated underneath Vestnesa Ridge during the PGM when the pan-Arctic ice sheet was formed with an estimated thickness of ~1500 to 2000 m on Svalbard (*41*, *42*). The result would have been a change in the subsurface stress regime, possibly creating migration pathways for deep-sourced fluids to migrate through the GHSZ (*5*) (Fig. 4A). On the basis of the seep carbonates and their ages alone, one cannot discriminate between the relatively slow plate tectonics (*5*) and the relatively fast glacial tectonics (*29*). Regardless, the clustering of the U-Th ages around ~148 ± 11 ka points to increased methane seepage limited to the PGM and possibly forebulge migration during the build-up of the pan-Arctic glaciation. Age constraints of glacial sediments onshore NW Svalbard (KII event; 165 ± 16 ka, 135 ± 11 ka, and 130 ± 8 ka) (*43*) confirm glaciation on Svalbard during the PGM in support of the forebulge hypothesis. Subsequent seepage quiescence following the forebulge collapse was likely due to the relative lower reservoir pore pressure in the seepage aftermath. Alternatively, the cores simply did not intersect the post-PGM seep carbonates. Further drilling will help address this sampling bias issue.

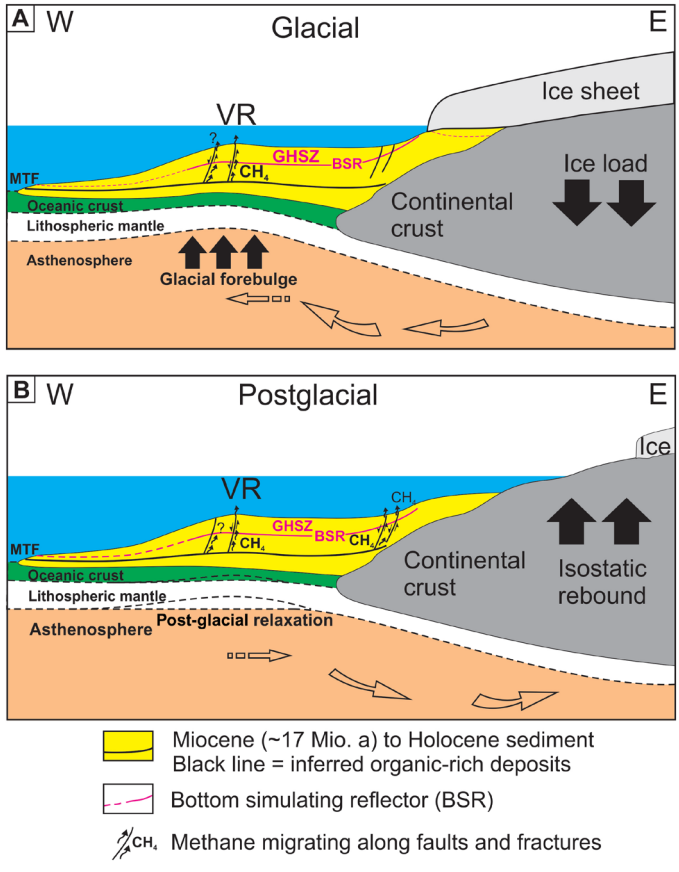

Fig. 4. Sketch illustrating the impact of glacial tectonics resulting from the waxing and waning of the Svalbard ice sheet on the subsurface fluid system of Vestnesa Ridge adapted from (*20*). (**A**) During ice sheet growth, horizontal mass transfer within the viscous asthenosphere (open arrows) facilitates migration of a glacial forebulge underneath Vestnesa Ridge. Sediment compaction due to vertical crustal adjustment (black arrows) causes reservoir overpressure. Reactivation of subvertical faults, connecting the gas reservoir to the seabed, provides migration pathways for deep-sourced fluids with methane (CH_4) through the GHSZ. (**B**) Post-glacial relaxation and associated mass transfer in the asthenosphere (open arrows) result in isostatic adjustment (black arrows) and fault reactivation, providing fluid migration pathways (not to scale). BSR, bottom simulating reflector, indicating the lower boundary of the GHSZ; MTF, Molly transform fault.

Downloaded from http://advances.sciencemag.org/ on August 9, 2019

Mid-Weichselian and post-LGM seepage

The second oldest seepage period identified in this area occurred during the mid Weichselian, ~50 to 40 ka. In the Northern Hemisphere, this period is characterized by long-term cooling reflected by advancing glaciers (Heinrich events), interrupted by pronounced millennial-scale warming episodes (Dansgaard-Oeschger events) (*44*, *45*). The GeoB21616-1 carbonate ages reveal seepage between Heinrich events H5 and H4 during relatively warmer climate when glaciers on Svalbard retreated (Fig. 3). On the basis of sedimentological and stratigraphic investigations onshore West Svalbard, deglaciation deposits have been dated between 60 and 35 ka (*46*, *43*). Coarsening upward sedimentary successions exposed on West Svalbard indicate rapid coastal uplift during isostatic adjustment following the glacial retreat (*46*). Rapid isostatic adjustment likely reactivated faults that connect to the deep reservoir, allowing fluid migration and seepage (Fig. 4B).

A similar scenario may account for the multiple LGM to Holocene seepage episodes revealed by the seabed carbonate ages (~20 to 5 ka; Fig. 3). Previously, it has been suggested that the post-LGM seepage was induced by fault and fracture reopening caused by glacioisostatic adjustment (*19*) of Svalbard. Likewise, glacial forebulge movement during ice sheet build-up may account for periodic enhanced seepage (Fig. 3). Marine sediments from the continental margin off West Svalbard indicate ice advance onto the shelf between ~22 and 18 ka, followed by ice retreat from the shelf around 14.8 ka and between 13 and 12 ka, with a minor ice advance around 12.4 ka (*47*). The seep carbonate ages indicate that the combined effects of glacial forebulge and isostatic rebound may have caused multiple seepage episodes in the LGM aftermath.

CONCLUSION

U-Th dates obtained from seabed and drill core–sampled seep carbonates from Vestnesa Ridge reveal methane seepage episodes around ~160 to 133 ka, ~50 to 40 ka, and ~20 to 5 ka. Seepage timing correlates with the waxing and waning of ice sheets. It is suggested that, besides lower glacial sea level, glacial tectonics mainly controlled seepage through repeated forebulge movement and isostatic adjustment. U-Th dating of cored seep carbonates provides bona fide evidence of pre-LGM seepage from a gas reservoir north of the Arctic Circle, corroborating the link between glacial-interglacial processes and deep-water methane release. It needs to be stressed that the results derived from only two shallow drill cores could reflect a spatial sampling bias, possibly not recovering the full seepage history. Lateral and deeper sediment coring could reveal a seepage history beyond the PGM and help test issues around sampling bias. Sampling seep carbonates by sediment coring above similar methane reservoirs in the Arctic has the potential to generate a chronology of past methane emissions over much of the Quaternary, thus providing additional constraints on local and global drivers of long-term seepage from deep-water methane reservoirs.

MATERIALS AND METHODS

Seabed sampling and observation

Authigenic seep carbonates were sampled from the seabed using the manipulator arms of the ROV Ægir 6000 during the R/V G.O. Sars expedition P1606 in 2016. Digital video cameras mounted on the ROV recorded seabed images during the dives.

Sediment coring and core sampling

Sediments were cored during the R/V Maria S. Merian expedition MSM57 in 2016 (*21*) using the portable deep-sea drill rig MARUM-MeBo70 (*48*). Seep carbonates were sampled from core sections as whole round samples and loose gravel. Whole rounds and gravel were split into working and archive halves using a wet rock saw.

Mineralogy, petrography, and stable isotope analysis

Quantitative mineralogical composition was determined by x-ray diffraction on microdrilled and bulk-rock powders of representative samples. Sample powders were analyzed using a Bruker D8 Advance diffractometer using Cu Kα radiation at a 2Θ scanning angle of 3° to 75° (step size of 0.02°, 1 s per step). Minerals were identified by automatic and manual peak search using the Bruker DIFFRAC EVA 3.1 software; quantification was performed applying Rietveld refinement with the TOPAS 5 software. Approximately 1.5-cm-thick slabs were cut from the rock samples; the slabs were embedded in epoxy resin. Thin sections (6.5 cm by 5 cm and 4.5 cm by 2.6 cm) were prepared from the embedded slabs and were examined using standard petrographic microscopy. Samples for stable carbon and oxygen isotopes were obtained from the cut slabs with a handheld microdrill. Powders were reacted with anhydrous phosphoric acid in a GasBench II preparation line; released CO_2 gas was analyzed with a Delta V Advantage isotope ratio mass spectrometer. The $\delta^{13}C$ and $\delta^{18}O$ values are reported in per mil (‰) relative to the VPDB standard. Reproducibility for $\delta^{13}C$ and $\delta^{18}O$ was estimated to be ±0.2‰.

U-Th chronology

A total of seven seabed and 16 core carbonates were selected for U-Th dating. The U-Th ages of a total of 58 void-filling aragonite cement samples were determined. Sample powders between 0.4 and 4.47 mg were obtained from epoxy-impregnated cut slabs using a handheld microdrill and a New Wave Research micromill. U and Th were separated, concentrated, and measured, as described in (*14*). Briefly, powders were digested in 8 M HNO_3 and centrifuged to separate the soluble carbonate fraction from insoluble detritus. The detritus was dissolved in a mixture of $HClO_4$:HF:HNO_3 [1:2:10 (v/v/v)], dried, and redissolved in 8 M HCl. U and Th were preconcentrated via iron coprecipitation and separated via column ion chromatography (*49*). Isotope ratios were measured with a Neptune Plus multicollector inductively coupled plasma mass spectrometer, equipped with an Aridus II desolvating nebulizer with a PFA nebulizer tip. Argon and nitrogen were used as carrying gases to minimize oxide formation. U-Th ages were calculated using an in-house spreadsheet, applying the ^{230}Th and ^{234}U decay constants of (*50*). ^{230}Th blanks of ca. 0.152 ± 0.029 fg were corrected for by subtracting the mean ^{230}Th signal of six unspiked total procedural blanks (15.8 ± 3.0 counts/s, 2σ) from the ^{230}Th signal intensity measured for each sample (300 to 5000 counts/s). U blanks amounting to 18.1 ± 8.8 pg of ^{238}U (2σ, $n = 12$) were corrected assuming a $^{238}U/^{235}U = 137.818$ (*51*) and a measured blank $^{234}U/^{235}U$ of 0.0144 ± 0.0027 (1σ, $n = 12$). Uncertainties on U and Th blank amounts were propagated into calculated age and initial ($^{234}U/^{238}U$) uncertainties. Initial Th correction was based on mean measured ($^{232}Th/^{238}U$), ($^{230}Th/^{238}U$), and ($^{234}U/^{238}U$) activity ratios of seep carbonate free Vestnesa Ridge sediment samples (data file S1). For subsamples with ($^{230}Th/^{232}Th$) lower than ~20, which are mainly from seep carbonates collected by ROV, the uncertainty budgets are dominated by contributions from the initial Th correction, while blank uncertainties account for up to

Downloaded from http://advances.sciencemag.org/ on August 9, 2019

20% and the measured isotope composition of the subsamples themselves account for up to 10% (fig. S13). For subsamples with (^{230}Th/^{232}Th) between 20 and 100, which come from a mixture of ROV-collected and cored seep carbonates, the impact of initial U-Th composition on the total age uncertainty budget decreases and the impact of sample U-Th composition increases with increasing (^{230}Th/^{232}Th), while blank amount uncertainties account for 10 to 70% (fig. S13). For subsamples with (^{230}Th/^{232}Th) greater than 100, which mainly come from cored seep carbonates, the age uncertainty budget is dominated by contributions from the measured subsample U-Th composition, while blank amount uncertainties account for 10 to 40% and those from the initial U-Th isotope composition are mostly negligible (fig. S13). U-Th ages are reported in thousand years before the present (ka BP; BP = before 1950). Samples with (^{230}Th/^{232}Th) activity ratios of ≤2 were rejected due to age uncertainties more than ±50%. The initial U isotope signature of seep carbonate tends to reflect seawater values or slight enrichment in ^{234}U relative to seawater if precipitation occurs under more restrictive conditions, and therefore, analyses where $(^{234}U/^{238}U)_{i\ sample} < 1.14$ or $(^{234}U/^{238}U)_{i\ sample} > 1.18$ were assumed to represent an open-system behavior with respect to U and/or Th and were rejected (data file S1). Of the 58 analyzed subsamples, 37 met the selection criterion for $(^{234}U/^{238}U)_i$, with 34 dates returning $(^{234}U/^{238}U)_i$ values within uncertainty of the mean modern seawater value of 1.145 (*52*) assuming an uncertainty of ±0.005. Alternative interpretations of data are possible based on variations in the selection criteria applied to calculated $(^{234}U/^{238}U)_i$ values and the U-Th isotope composition underpinning the initial Th correction. As seep carbonate-free sediment samples from Vestnesa Ridge displayed a wide range of (^{230}Th/^{238}U) and (^{232}Th/^{238}U) values (1.10 to 1.90 and 1.03 to 1.93, respectively), we evaluated the impact of initial Th corrections based on the mean of all measured sediment samples, the mean of the most/least Th-enriched sediment samples, and an interpolated sediment U-Th isotope composition based on data from the U.S. Atlantic margin (*53*) on calculated ages. These alternative interpretations are explored in fig. S14, along with the impact of different initial U-Th isotope compositions on calculated initial (^{234}U/^{238}U) values, and do not have an impact on the conclusions drawn in this study.

SUPPLEMENTARY MATERIALS

Supplementary material for this article is available at http://advances.sciencemag.org/cgi/content/full/5/8/eaaw1450/DC1

Fig. S1. Area seabed photographs at Lomvi and Lunde pockmarks.
Fig. S2. Scanned images of archive half sections and description of core GeoB21616-1.
Fig. S3. Scanned images of archive half sections and description of core GeoB21637-1.
Fig. S4. Scans of cut slabs from seabed carbonates with detailed U-Th sample locations and ages (ka BP ± 2σ).
Fig. S5. Scans of thin-section slabs impregnated in epoxy resin with detailed U-Th sample locations and ages in ka BP ± 2σ.
Fig. S6. Scans of thin-section slabs impregnated in epoxy resin with detailed U-Th sample locations and ages in ka BP ± 2σ.
Fig. S7. Thin-section micrographs of seabed samples.
Fig. S8. Thin-section micrographs of core samples (all cross-polarized light; pore space appears black).
Fig. S9. Range of (^{230}Th/^{232}Th) versus (^{238}U/^{232}Th) from this study compared to other seep carbonate literature.
Fig. S10. Calculated U-Th ages without dates excluded based on screening criteria plotted against sampling depth.
Fig. S11. Seep carbonate ages and respective relative sea level.
Fig. S12. Cross plots of carbonate carbon and oxygen stable isotope compositions (in ‰ VPDB).
Fig. S13. Breakdown of the uncertainty budget of calculated seep carbonate ages.
Fig. S14. Alternative interpretation of U-Th data.
Table S1. Mineralogical compositions (weight %) of seabed sampled carbonates.
Table S2. Mineralogical compositions (weight %) of core carbonates.
Data file S1. Spreadsheet containing U-Th isotopic data of seep carbonates and seep carbonate-free sediment, as well as calculated U-Th ages and carbonate $\delta^{13}C$ and $\delta^{18}O$ values.
References (*55*–*57*)

REFERENCES AND NOTES

1. D. L. Gauthier, K. J. Bird, R. R. Charpentier, A. Grantz, D. W. Houseknecht, T. R. Klett, T. E. Moore, J. K. Pitman, C. J. Schenk, J. H. Schuenemeyer, K. Sørensen, M. E. Tennyson, Z. C. Valin, C. J. Wandrey, Assessment of undiscovered oil and gas in the Arctic. *Science* **324**, 1175–1179 (2009).
2. I. S. Stewart, J. Sauber, J. Rose, Glacio-seismotectonics: Ice sheets, crustal deformation and seismicity. *Quat. Sci. Rev.* **19**, 1367–1389 (2000).
3. H. Patton, A. Hubbard, K. Andreassen, A. Auriac, P. L. Whitehouse, A. P. Stroeven, C. Shackleton, M. Winsborrow, J. Heyman, A. M. Hall, Deglaciation of the Eurasian ice sheet complex. *Quat. Sci. Rev.* **169**, 148–172 (2017).
4. C. D. Ruppel, J. D. Kessler, The interaction of climate change and methane hydrates. *Rev. Geophys.* **55**, 126–168 (2017).
5. A. Plaza-Faverola, S. Bünz, J. E. Johnson, S. Chand, J. Knies, J. Mienert, P. Franek, Role of tectonic stress in seepage evolution along the gas hydrate-charged Vestnesa Ridge, Fram Strait. *Geophys. Res. Lett.* **42**, 733–742 (2015).
6. E. Suess, Marine cold seeps and their manifestations: Geological control, biogeochemical criteria and environmental conditions. *Int. J. Earth Sci.* **103**, 1889–1916 (2014).
7. A. Boetius, K. Ravenschlag, C. J. Schubert, D. Rickert, F. Widdel, A. Gieseke, R. Amann, B. B. Jørgensen, U. Witte, O. Pfannkuche, A marine microbial consortium apparently mediating anaerobic oxidation of methane. *Nature* **407**, 623–626 (2000).
8. W. Reeburgh, Oceanic methane biogeochemistry. *Chem. Rev.* **107**, 486–513 (2007).
9. E. J. Beal, C. H. House, V. J. Orphan, Manganese- and iron-dependent marine methane oxidation. *Science* **325**, 184–187 (2009).
10. S. Ritger, B. Carson, E. Suess, Methane-derived authigenic carbonates formed by subduction-induced pore-water expulsion along the Oregon/Washington margin. *Geol. Soc. Am. Bull.* **98**, 147–156 (1987).
11. G. Aloisi, I. Bouloubassi, S. K. Heijs, R. Pancost, C. Pierre, J. S. Sinninghe Damsté, J. C. Gottschal, L. J. Forney, J.-M. Rouchy, CH_4–consuming microorganisms and the formation of carbonate crusts at cold seeps. *Earth Planet. Sci. Lett.* **203**, 195–203 (2002).
12. B. M. A. Teichert, A. Eisenhauer, G. Bohrmann, A. Haase-Schramm, B. Bock, P. Linke, U/Th systematics and ages of authigenic carbonates from Hydrate Ridge, Cascadia Margin: Recorders of fluid flow variations. *Geochim. Cosmochim. Acta* **67**, 3845–3857 (2003).
13. C. Berndt, T. Feseker, T. Treude, S. Krastel, V. Liebetrau, H. Niemann, V. J. Bertics, I. Dumke, K. Dünnbier, B. Ferré, C. Graves, F. Gross, K. Hissmann, V. Hühnerbach, S. Krause, K. Lieser, J. Schauer, L. Steinle, Temporal constraints on hydrate-controlled methane seepage off Svalbard. *Science* **343**, 284–287 (2014).
14. A. Crémière, A. Lepland, S. Chand, D. Sahy, D. J. Condon, S. R. Noble, T. Martma, T. Thorsnes, S. Sauer, H. Brunstad, Timescales of methane seepage on the Norwegian margin following collapse of the Scandinavian Ice Sheet. *Nat. Commun.* **7**, 11509 (2016).
15. K. Andreassen, A. Hubbard, M. Winsborrow, H. Patton, S. Vadakkepuliyambatta, A. Plaza-Faverola, E. Gudlaugsson, P. Serov, A. Deryabin, R. Mattingsdal, J. Mienert, S. Bünz, Massive blow-out craters formed by hydrate-controlled methane expulsion from the Arctic seafloor. *Science* **356**, 948–953 (2017).
16. S. Mau, M. Römer, M. E. Torres, I. Bussmann, T. Pape, E. Damm, P. Geprägs, P. Wintersteller, C.-W. Hsu, M. Loher, G. Bohrmann, Widespread methane seepage along the continental margin off Svalbard–from Bjørnøya to Kongsfjorden. *Sci. Rep.* **7**, 42997 (2017).
17. S. Hustoft, S. Bünz, J. Mienert, S. Chand, Gas hydrate reservoir and active methane-venting province in sediments on < 20 Ma young oceanic crust in the Fram Strait, offshore NW-Svalbard. *Earth Planet. Sci. Lett.* **284**, 12–24 (2009).
18. S. Bünz, S. Polyanov, S. Vadakkepuliyambatta, C. Consolaro, J. Mienert, Active gas venting through hydrate-bearing sediments on the Vestnesa Ridge, offshore W-Svalbard. *Mar. Geol.* **332–334**, 189–197 (2012).
19. A. Schneider, G. Panieri, A. Lepland, C. Consolaro, A. Crémière, M. Forwick, J. E. Johnson, A. Plaza-Faverola, S. Sauer, J. Knies, Methane seepage at Vestnesa Ridge (NW Svalbard) since the Last Glacial Maximum. *Quat. Sci. Rev.* **193**, 98–117 (2018).
20. J. Knies, M. Daszinnies, A. Plaza-Faverola, S. Chand, Ø. Sylta, S. Bünz, J. E. Johnson, R. Mattingsdal, J. Mienert, Modelling persistent methane seepage offshore western Svalbard since early Pleistocene. *Mar. Pet. Geol.* **91**, 800–811 (2018).
21. G. Bohrmann, F. Ahrlich, M. Bergenthal, S. Bünz, R. Düßmann, C. Ferreira, T. Freudenthal, S. Fröhlich, K. Hamann, W.-L. Hong, C.-W. Hsu, J. Johnson, K. Kaszemeik, A. Kausche, T. Klein, M. Lange, A. Lepland, J. Malnati, S. Meckel, B. Meyer-Schack, K. Noorlander, G. Panieri, T. Pape, M. Reuter, M. Riedel, U. Rosiak, C. Schmidt, W. Schmidt, C. Seiter, G. Spagnoli, A. Stachowski, N. Stange, K. Wallmann, P. Wintersteller, D. Wunsch, H. Yao, *R/V MARIA S. MERIAN Cruise Report MSM57, Gas Hydrate Dynamics at the Continental*

Downloaded from http://advances.sciencemag.org/ on August 9, 2019

Margin of Svalbard, Reykjavik–Longyearbyen–Reykjavik, 29 July–07 September 2016 (MARUM–Zentrum für Marine Umweltwissenschaften, Fachbereich Geowissenschaften, Bremen University, Bremen, 2017).
22. G. Panieri, S. Bünz, D. J. Fornari, J. Escartin, P. Serov, P. Jansson, M. E. Torres, J. E. Johnson, W. Hong, S. Sauer, R. Garcia, N. Gracias, An integrated view of the methane system in the pockmarks at Vestnesa Ridge, 79°N. *Mar. Geol.* **390**, 282–300 (2017).
23. G. Bayon, G. M. Henderson, M. Bohn, U–Th stratigraphy of a cold seep carbonate crust. *Chem. Geol.* **260**, 47–56 (2009).
24. D. Feng, H. H. Roberts, H. Cheng, J. Peckmann, G. Bohrmann, R. L. Edwards, D. Chen, U/Th dating of cold-seep carbonates: An initial comparison. *Deep Sea Res. Part II Top. Stud. Oceanogr.* **57**, 2055–2060 (2010).
25. A. Crémière, G. Bayon, E. Ponzevera, C. Pierre, Paleo–environmental controls on cold seep carbonate authigenesis in the sea of Marmara. *Earth Planet. Sci. Lett.* **376**, 200–211 (2013).
26. A. Crémière, A. Lepland, S. Chand, D. Sahy, K. Kirsimäe, M. Bau, M. J. Whitehouse, S. R. Noble, T. Martma, T. Thorsnes, H. Brunstad, Fluid source and methane-related diagenetic processes recorded in cold seep carbonates from the Alvheim channel, central North Sea. *Chem. Geol.* **432**, 16–33 (2016).
27. A. Plaza-Faverola, S. Bünz, J. Mienert, Repeated fluid expulsion through sub-seabed chimneys offshore Norway in response to glacial cycles. *Earth Planet. Sci. Lett.* **305**, 297–308 (2011).
28. V. Riboulot, A. Cattaneo, N. Sultan, S. Garziglia, S. Ker, P. Imbert, M. Voisset, Sea-level change and free gas occurrence influencing a submarine landslide and pockmark formation and distribution in deepwater Nigeria. *Earth Planet. Sci. Lett.* **375**, 78–91 (2013).
29. R. M. Thorson, Glacial tectonics: A deeper perspective. *Quat. Sci. Rev.* **19**, 1301–1398 (2000).
30. T. Himmler, D. Birgel, G. Bayon, T. Pape, L. Ge, G. Bohrmann, J. Peckmann, Formation of seep carbonates along the Makran convergent margin, northern Arabian Sea and a molecular and isotopic approach to constrain the carbon isotopic composition of parent methane. *Chem. Geol.* **415**, 102–117 (2015).
31. M. J. Whiticar, Carbon and hydrogen isotope systematics of bacterial formation and oxidation of methane. *Chem. Geol.* **161**, 291–314 (1999).
32. J. Greinert, G. Bohrmann, E. Suess, Gas hydrate associated carbonates and methane-venting at Hydrate Ridge; Classification, distribution, and origin of authigenic lithologies. *Geoph. Monog. Series* **124**, 99–113 (2001).
33. D. W. Davidson, D. G. Leaist, R. Hesse, Oxygen-18 enrichment in the water of a clathrate hydrate. *Geochim. Cosmochim. Acta* **47**, 2293–2295 (1983).
34. C. Hensen, K. Wallmann, M. Schmidt, C. R. Ranero, E. Suess, Fluid expulsion related to mud extrusion off Costa Rica—A window to the subducting slab. *Geology* **32**, 201–204 (2004).
35. R. Luff, K. Wallmann, G. Aloisi, Numerical modeling of carbonate crust formation at cold vent sites: Significance for fluid and methane budgets and chemosynthetic biological communities. *Earth Planet. Sci. Lett.* **221**, 337–353 (2004).
36. F. Zhang, H. Xu, H. Konishi, J. M. Kemp, E. E. Roden, Z. Shen, Dissolved sulfide-catalyzed precipitation of disordered dolomite: Implications for the formation mechanism of sedimentary dolomite. *Geochim. Cosmochim. Acta* **97**, 148–165 (2012).
37. M. Hovland, M. R. Talbot, H. Qvale, S. Olaussen, L. Aasberg, Methane-related carbonate cements in pockmarks of the North Sea. *J. Sediment. Petrol.* **57**, 881–892 (1987).
38. E. J. Rohling, F. D. Hibbert, F. H. Williams, K. M. Grant, G. Marino, G. L. Foster, R. Hennekam, G. J. de Lange, A. P. Roberts, J. Yu, J. M. Webster, Y. Yokoyama, Differences between the last two glacial maxima and implications for ice-sheet, $\delta^{18}O$, and sea-level reconstructions. *Quat. Sci. Rev.* **176**, 1–28 (2017).
39. A. Plaza-Faverola, S. Vadakkepuliyambatta, W.-L. Hong, J. Mienert, S. Bünz, S. Chand, J. Greinert, Bottom-simulating reflector dynamics at Arctic thermogenic gas provinces: An example from Vestnesa Ridge, offshore west Svalbard. *J. Geophys. Res. Solid Earth* **122**, 4089–4105 (2017).
40. W. Fjeldskaar, The amplitude and decay of the glacial forebulge in Fennoscandia. *Norsk Geol. Tidsskr.* **74**, 2–8 (1994).
41. F. Colleoni, G. Krinner, M. Jakobsson, V. Peyaud, C. Ritz, Influence of regional parameters on the surface mass balance of the Eurasian ice sheet during the peak Saalian (140 kya). *Glob. Planet. Change* **68**, 132–148 (2009).
42. M. Jakobsson, J. Nilsson, L. Anderson, J. Backman, G. Björk, T. M. Cronin, N. Kirchner, A. Koshurnikov, L. Mayer, R. Noormets, M. O'Regan, C. Stranne, R. Ananiev, N. Barrientos Macho, D. Cherniykh, H. Coxall, B. Eriksson, T. Flodén, L. Gemery, Ö. Gustafsson, K. Jerram, C. Johansson, A. Khortov, R. Mohammad, I. Semiletov, Evidence for an ice shelf covering the central Arctic Ocean during the penultimate glaciation. *Nat. Commun.* **7**, 10356 (2016).
43. H. Alexanderson, M. Henriksen, H. T. Ryen, J. Y. Landvik, G. Peterson, 200 ka of glacial events in NW Svalbard: An emergence cycle facies model and regional correlations. *Arktos* **4**, (2018).
44. J. T. Andrews, A. H. L. Voelker, "Heinrich events" (& sediments): A history of terminology and recommendations for future usage. *Quat. Sci. Rev.* **187**, 31–40 (2018).
45. G. Bond, W. Broecker, S. Johnsen, J. McManus, L. Labeyrie, J. Jouzel, G. Bonani, Correlation between climate records from North Atlantic sediments and Greenland ice. *Nature* **356**, 143–147 (1993).
46. J. Mangerud, T. Dokken, D. Hebbeln, B. Heggen, Ó. Ingólfsson, J. Y. Landvik, V. Mejdahl, J. I. Svendsen, T. O. Vorren, Fluctuations of the Svalbard–Barents Sea ice sheet during the last 150 000 years. *Quat. Sci. Rev.* **17**, 11–42 (1998).
47. A. Elverhøi, E. S. Andersen, T. Dokken, D. Hebbeln, R. Spielhagen, J. I. Svendsen, M. Sørflaten, A. Rørnes, M. Hald, C. F. Forsberg, The growth and decay of the late Weichselian ice sheet in western Svalbard and adjacent areas based on provenance studies of marine sediments. *Quat. Res.* **44**, 306–316 (1995).
48. T. Freudenthal, G. Wefer, Drilling cores on the sea floor with the remote-controlled sea floor drilling rig MeBo. *Geosci. Instrum. Method. Data Syst.* **2**, 329–337 (2013).
49. R. L. Edwards, J. H. Chen, G. J. Wasserburg, ^{238}U–^{234}U–^{230}Th–^{232}Th systematics and the precise measurement of time over the past 500,000 years. *Earth Planet. Sci. Lett.* **81**, 175–192 (1987).
50. H. Cheng, R. L. Edwards, C.-C. Shen, V. J. Polyak, Y. Asmerom, J. Woodhead, J. Hellstrom, Y. Wang, X. Kong, C. Spötl, X. Wang, E. C. Alexander Jr., Improvements in ^{230}Th dating, ^{230}Th and ^{234}U half-life values, and U–Th isotopic measurements by multi-collector inductively coupled plasma mass spectrometry. *Earth Planet. Sci. Lett.* **371–372**, 82–91 (2013).
51. J. Hiess, D. J. Condon, N. McLean, S. R. Noble, $^{238}U/^{235}U$ systematics in terrestrial uranium-bearing minerals. *Science* **335**, 1610–1614 (2012).
52. P. M. Chutcharavan, A. Dutton, M. J. Ellwood, Seawater $^{234}U/^{238}U$ recorded by modern and fossil corals. *Geochim. Cosmochim. Acta* **224**, 1–17 (2018).
53. N. G. Prouty, D. Sahy, C. D. Ruppel, E. B. Roark, D. Condon, S. Brooke, S. W. Ross, A. W. J. Demopoulos, Insights into methane dynamics from analysis of authigenic carbonates and chemosynthetic mussels at newly-discovered Atlantic Margin seeps. *Earth Planet. Sci. Lett.* **449**, 332–344 (2016).
54. M. Jakobsson, L. Mayer, B. Coakley, J. A. Dowdeswell, S. Forbes, B. Fridman, H. Hodnesdal, R. Noormets, R. Pedersen, M. Rebesco, H. W. Schenke, Y. Zarayskaya, D. Accettella, A. Armstrong, R. M. Anderson, P. Bienhoff, A. Camerlenghi, I. Church, M. Edwards, J. V. Gardner, J. K. Hall, B. Hell, O. Hestvik, Y. Kristoffersen, C. Marcussen, R. Mohammad, D. Mosher, S. V. Nghiem, M. T. Pedrosa, P. G. Travaglini, P. Weatherall, The International Bathymetric Chart of the Arctic Ocean (IBCAO) Version 3.0. *Geophys. Res. Lett.* **39**, L12609 (2012).
55. S.-T. Kim, J. R. O'Neil, C. Hillaire-Marcel, A. Mucci, Oxygen isotope fractionation between synthetic aragonite and water: Influence of temperature and Mg^{2+} concentration. *Geochim. Cosmochim. Acta* **71**, 4704–4715 (2007).
56. M. M. Ezat, T. L. Rassmussen, J. Groeneveld, Persistent intermediate water warming during cold stadials in the southeastern Nordic seas during the past 65 k.y. *Geology* **42**, 663–666 (2014).
57. N. Lang, E. W. Wolff, Interglacial and glacial variability from the last 800 ka in marine, ice and terrestrial archives. *Clim. Past* **7**, 361–380 (2011).

Acknowledgments: Professional support at sea by the masters and crews during expeditions on R/V G.O. Sars (P1606) and R/V Maria S. Merian (MSM57) and the skillful works of the ROV Ægir 6000 team (University of Bergen) and the MARUM-MeBo70 team (University of Bremen) are greatly acknowledged. We thank J. Schönenberger (Geological Survey of Norway) and D. Wagner (British Geological Survey) for laboratory support and S. Noble (British Geological Survey) for discussion on ^{230}Th blanks. Seabed photographs in fig. S1 were taken with the ROV during R/V G.O. Sars expedition P1606 in July 2016. Thoughtful comments by three reviewers helped to improve the manuscript. **Funding:** Expedition MSM57 onboard R/V Maria S. Merian was funded by the German Research Foundation (DFG) and funds from the Centre for Arctic Gas Hydrate, Environment and Climate (CAGE) and Equinor ASA. The study was supported by the CAGE and the Research Council of Norway through its Centres of Excellence scheme (grant no. 223259) and the Petromaks2 NORCRUST project (grant no. 255150). **Author contributions:** T.H. and A.L. conceived the study. T.H. prepared isotope samples. D.S. produced U-Th data with input from D.J.C. T.M. performed stable isotope analyses. G.B., S.B., A.P.-F., J.K., and A.L. co-organized expeditions and sampling at sea. T.H. wrote the manuscript with input from all co-authors. **Competing interests:** All authors declare that they have no competing interests. **Data and materials availability:** All data needed to evaluate the conclusions in the paper are present in the paper and/or the Supplementary Materials. Additional data related to this paper may be requested from the authors.

Submitted 21 November 2018
Accepted 28 June 2019
Published 7 August 2019
10.1126/sciadv.aaw1450

Citation: T. Himmler, D. Sahy, T. Martma, G. Bohrmann, A. Plaza-Faverola, S. Bünz, D. J. Condon, J. Knies, A. Lepland, A 160,000-year-old history of tectonically controlled methane seepage in the Arctic. *Sci. Adv.* **5**, eaaw1450 (2019).

Downloaded from http://advances.sciencemag.org/ on August 9, 2019

Science Advances

A 160,000-year-old history of tectonically controlled methane seepage in the Arctic

Tobias Himmler, Diana Sahy, Tõnu Martma, Gerhard Bohrmann, Andreia Plaza-Faverola, Stefan Bünz, Daniel J. Condon, Jochen Knies and Aivo Lepland

Sci Adv **5** (8), eaaw1450.
DOI: 10.1126/sciadv.aaw1450

ARTICLE TOOLS http://advances.sciencemag.org/content/5/8/eaaw1450

SUPPLEMENTARY MATERIALS http://advances.sciencemag.org/content/suppl/2019/08/05/5.8.eaaw1450.DC1

REFERENCES This article cites 55 articles, 9 of which you can access for free
http://advances.sciencemag.org/content/5/8/eaaw1450#BIBL

PERMISSIONS http://www.sciencemag.org/help/reprints-and-permissions

Use of this article is subject to the Terms of Service

Science Advances (ISSN 2375-2548) is published by the American Association for the Advancement of Science, 1200 New York Avenue NW, Washington, DC 20005. 2017 © The Authors, some rights reserved; exclusive licensee American Association for the Advancement of Science. No claim to original U.S. Government Works. The title *Science Advances* is a registered trademark of AAAS.

Downloaded from http://advances.sciencemag.org/ on August 9, 2019